Letter

Measurement of the total neutron cross section on argon in the 20 to 70 keV energy range

S. Andringa,[1] Y. Bezawada,[2] T. Erjavec,[2] J. He,[2] J. Huang,[2] P. Koehler,[3] M. Mocko,[3] M. Mulhearn,[2] L. Pagani,[2] E. Pantic,[2] L. Pickard,[2] R. Svoboda,[2] J. Ullmann,[3] and J. Wang[2,4]
(ARTIE Collaboration)
[1]*Laboratório de Instrumentação e Física Experimental de Partículas (LIP), Avenida Prof. Gama Pinto 2, 1649-003 Lisboa, Portugal*
[2]*Department of Physics and Astronomy, University of California at Davis, Davis, California 95616, USA*
[3]*Physics Division, Los Alamos National Laboratory, Los Alamos, New Mexico 87545, USA*
[4]*Physics Department, South Dakota School of Mines and Technology, Rapid City, South Dakota 57701, USA*

(Received 30 December 2022; accepted 12 June 2023; published 7 July 2023)

The cross section for neutron interactions on argon is an important design and operational parameter for a number of neutrino, dark matter, and neutrinoless double beta decay experiments which use liquid argon as a detection or shielding medium. There is a discrepancy between the evaluated total cross section in the 20 to 70 keV neutron kinetic energy region given in the ENDF database and a single measurement conducted by an experiment with a thin target (0.2 atoms/b) optimized for higher cross sections. This gives rise to significant uncertainty in the interaction length of neutrons in liquid argon. This discrepancy is now resolved by new results presented here from the Argon Resonance Transport Interaction Experiment (ARTIE), a thick target experiment (3.3 atoms/b) optimized for the small cross sections in this energy region.

DOI: 10.1103/PhysRevC.108.L011601

Liquid argon (LAr) is used in a wide range of particle physics experiments investigating neutrinos [1–4], dark matter [5,6], and neutrinoless double beta decay [7,8]. Achieving the scientific objectives sought by these experiments relies on understanding the transport of neutrons through LAr at a level of precision which has only recently emerged as a critical experimental requirement.

Recent studies have shown that understanding the behavior of neutrons presents a special challenge in liquid-argon-based experiments [9–11].

The neutron-argon total cross section from the ENDF [12] evaluation has a destructive interference feature at 57 keV, which appears as a dip in the cross section around this energy, where interaction length in LAr, for a natural abundance of isotopes, is 30 m. This is important, as at this energy scale neutrons only lose a small fraction of their kinetic energy in single elastic collisions with relatively massive argon nuclei. Thus, even neutrons with kinetic energy well above 57 keV have a significant probability of reaching the low cross section region with the resulting long interaction length. The results of the most recent previous measurement [13], contained in the EXFOR database [14], are inconsistent with ENDF evaluation in the region of this feature, with an inferred interaction length of 4.2 m. This discrepancy makes it impossible to reliably predict the performance of LAr in transporting and/or shielding neutrons. This is especially important for the DUNE experiment [15,16] now under construction.

This paper presents the results of the Argon Resonant Transport Interaction Experiment (ARTIE), which was designed specifically to resolve the neutron cross section discrepancy.

Experimental method. The transmission through a target in a neutron beam $T(E)$ is defined as the fraction of neutrons in a medium which pass through a distance d without scattering. This is related to the cross section by the equation

$$\sigma(E) = -\frac{m}{\rho_{\text{eff}}\, d} \ln T(E), \tag{1}$$

where m is the mass of an argon atom, d is the target thickness, and ρ_{eff} is the effective density. The ARTIE target was designed with a thickness approximately twenty times larger than used in Ref. [13]. Thus, the inconsistent cross section values reported by ENDF and Ref. [13] result in a 20% difference in $T(E)$ at the dip energy.

While well suited to the dip region, the target becomes essentially opaque at energies where the cross section is higher, restricting our energy region ofinterest (ROI) to 20 to 70 keV. To make the measurement, Flight Path 13 (FP13) at the Lujan Neutron Scattering Center [17] was used. FP13 has a total flight path of about 64 meters, allowing for excellent time of flight (TOF) energy resolution up to several hundred keV.

The ARTIE experimental configuration is shown in Fig. 1. The ARTIE target consisted of a column of LAr of length 168 cm and diameter 25 mm, held at atmospheric pressure, and contained in a vessel constructed from standard components.

The target was inserted into FP13 at a distance of about 31 m from the upper-tier liquid hydrogen moderator of the proton-accelerator-driven pulsed neutron source.

The proton beam current (proportional to the resulting neutron flux) was monitored by a current transformer (CT), with the integral output recorded every minute for relative beam normalization.

The ARTIE neutron detector was located at the end of the beam line, about 30 m downstream of the target, and consisted of a 9 cm diameter by 1 mm thick ^{6}Li-glass scintillator,

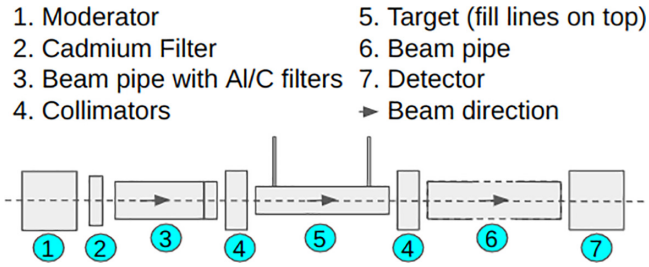

FIG. 1. Configuration of the beam line elements. (1) Mark III LANSCE target and moderator. (2) Cadmium filter for suppression of thermal neutrons. (3) ≈30 m beam pipe where carbon and aluminum filters were mounted. (4) Brass collimators. (5) ARTIE target. (6) ≈30 m beam pipe. (7) ^{6}Li-glass detector at 64 m followed by beam dump.

viewed edge on by two RCA 8854 five-inch photomultiplier tubes (PMTs). A triggered event was defined as a pulse above threshold in either PMT. The data acquisition system (DAQ) recorded the time and integrated PMT charge for each trigger.

Two-inch-thick brass cylinders with 6 mm holes in the center were used to collimate the beam through the target. Two collimators were located upstream of the target, and two downstream. These constrained the beam to the center of the 25 mm diameter target, and produced a beam spot with an 8 cm diameter at the 9 cm diameter neutron detector. Final alignment of the collimators was performed by first maximizing the DAQ-reported event rate. Collimators were then fine tuned in order to produce a symmetric, fully contained image on storage-phosphor image plates at the detector location.

For insulation, the target was covered with a rigid foam designed for cryogenic applications. Near each end an upward opening feeds into commercial nalgene dewars. As argon boiled in the target, gaseous argon (GAr) vented through the openings and was replaced by LAr from the dewars. During operation, dewars were refilled about once per hour to ensure that the target remained full. Data were collected during a two-week period, with most runs being in either *target-in* (LAr fill) or *target-out* (GAr fill) mode. The use of GAr during target-out runs was accounted for by defining the effective target density as $\rho_{\text{eff}} = \rho_{\text{in}} - \rho_{\text{out}}$. The transmission was then experimentally determined as

$$T(E) = \frac{N_{\text{in}}(E) - B_{\text{in}}}{N_{\text{out}}(E) - B_{\text{out}}} \frac{Q_{\text{out}}}{Q_{\text{in}}}, \tag{2}$$

where $N_{\text{in/out}}$ is the number of neutrons observed during target-in/out runs, $Q_{\text{in/out}}$ is the time-integrated beam current from the CT monitor, and $B_{\text{in/out}}$ is the experimentally determined background rate.

The collected data were subjected to both run quality and individual event selection cuts. First, to minimize the impact of potential nonlinearity between the CT sensor and the neutron beam intensity, the analysis only included the 95% of collected data taken while the CT was near the maximum value. Second, data taken around the time of target filling were rejected since during these times a roughly 30% excursion in the beam-intensity normalized neutron event rate was observed, which we surmise was caused by the unavoidable spilling of LAr vapor into the brass collimators from the filling dewar located above them. The rate returned to the nominal value about 15 minutes after the end of the fill. Thus, these filling times were removed from the analysis by requiring that the postfill rate return to at least 95% of the prefill plateau value. This cut removed about 12% of the target-in data. Third, both detector PMTs were required to have pulses within a 100 ns coincidence window, and to pass a cut which removed retriggered events (i.e., two triggers from a single event). This last cut removed a negligible number of actual signal events. Following these cuts, there were 197 000 events recorded in the ROI for target-in runs, and 85 000 for target-out.

Energy calibration. The neutron detector recorded a time (t_n) and the proton beam pulse provided a start time (t_0). Together these gave a TOF which was used to determine the velocity (v) and hence the kinetic energy (E) of each event. These times were corrected for the average time a neutron scattered inside the moderator (t_{mod}), usually referred to as the *moderator function* (MF). The MF had been previously determined for LANSCE via Monte Carlo simulation [18]. In the ROI this correction is typically 1–2% with a smearing of roughly 10% about the mean.

The velocity v is then a function of the TOF $t \equiv t_n - t_0$:

$$v(t) = \frac{L_{\text{fit}}}{t - t_{\text{mod}}(t) + t_{\text{fit}}}, \tag{3}$$

where L_{fit} and t_{fit} were parameters determined by fitting LAr data to known resonances of aluminum and cadmium (both present in the beam line) and argon. The best fit value of L_{fit} was 63.82 ± 0.06 m, which agrees well with physical measurements made along the beam line. The parameter t_{fit} (best fit 420 ± 29 ns) accounted for time delays in the detector, cables, and DAQ, as well as any residual difference between the actual and simulated moderator response. In addition to the MF time-smearing, the incident triangular-shaped neutron pulse had a FWHM of 125 ns which led to a 53 ns uncertainty in t_0. These two factors dominated the energy resolution.

Target density. Since the LAr in the target was always slightly boiling, there was always a small fraction of GAr present, which affected the overall target density. Thus, a separate experiment to directly measure the density of the liquid-gas mixture *in situ* was performed. The mass of the target assembly (M) as a function of dewar liquid height (h) is given by $M(h) = M_0 + (\rho_{\text{eff}} - \rho_{\text{air}})V(h)$, where ρ_{eff} is the effective density of the argon mixture, ρ_{air} is the density of air, M_0 is the mass of the empty target, and $V(h)$ is the volume of the target as a function of liquid height. M_0 was measured using a precision scale (± 1 g in the range of the roughly 25 kg target assembly mass), and $V(h)$ was determined by filling the target with known amounts of water and noting the level on a steel ruler inside the dewar. The dry, empty target was then filled with liquid argon while sitting on the precision scale. During the subsequent boil off, a camera was used to simultaneously record the scale mass M and the liquid level h, which were then analyzed to give $M(h)$. The observed boil off rate of 1.56 l/hr during this test was consistent with that observed during the actual neutron beam runs. A target-in density of $\rho_{\text{in}} = 1.318 \pm 0.017$ g/cm^3 was obtained, which included a correction for ice buildup on the target.

This is 5.9% lower than the nominal density [19] of pure liquid phase, and implies that this fraction of argon gas was mixed in the target during the beam runs. This resulted in an effective density $\rho_{\text{eff}} = 3.30 \pm 0.04$ atoms/b. Additionally, a 1.3% upward adjustment in LAr density was made to account for the difference in density at the altitude of Los Alamos (2300 m) as compared to the laboratory where the density test was performed (16 m). The uncertainty in the density measurement was taken into account when calculating the overall experimental uncertainty.

Backgrounds. Measurement of the transmission from Eq. (2) relied on subtracting background events, especially for the GAr runs. The two major backgrounds were (i) scattered neutrons from times earlier than the ROI that hit the detector at random later times, and (ii) gammas from neutron capture on water in the moderator. Other backgrounds such as "wrap-around" neutrons, prompt moderator gammas, and random backgrounds from other beam lines were determined to be insignificant.

To measure these major backgrounds, a standard technique [24] that utilizes resonances that scatter or absorb nearly all incident neutrons was used. Many beam line components are made of aluminum, and thus there are aluminum resonance features present in the data at 5.9, 35, and 88 keV. In addition, dedicated runs were made with an additional 2.54 cm aluminum filter inserted into the beam to further enhance these features. The background was then extracted at the resonance energy by subtracting the expected counts given the calculated aluminum transmission from the observed counts, given by

$$B_{\text{out}}(E) = \frac{N_{\text{in},f}(E) - R_{\text{in},f/\text{out}}(E)\, N_{\text{out}}(E)\, T(E)}{R_{\text{in},f/\text{out}}(E)[1 - T(E)]}, \quad (4)$$

where $T(E)$ is the calculated effective transmission of neutrons with the aluminum filter, $N(E)$ are the counts in the bins at the resonance dips at 5.9, 35, and 88 keV for the filtered case (in, f) and unfiltered case (out), and $R_{\text{in},f/\text{out}}(E)$ is the ratio of filtered background to the unfiltered background. This ratio is introduced to correct background reduction due to filter attenuation.

Both the random-scatter neutron and the moderator capture gammas are seen to be nearly flat in time within our ROI [22] for our neutron beam. As the filter attenuation effect is non-negligible for the 2.54 cm aluminum filter, it is corrected by $R_{\text{in},f/\text{out}}(E) = B_{\text{in},f}(E)/B_{\text{out}}(E)$ using an external measurement of the background components from [22] and from private communication with the authors [23]. The ratio is $R_{\text{in},f/\text{out}}(E_{\text{ROI}}) = 0.755^{+0.021}_{-0.004}$, with total uncertainties determined by applying Eq. (4) for situations when $B_{\text{out}}(E)$ consists entirely of gammas or neutrons.

For LAr fill runs, gammas from the moderator were heavily suppressed due to target thickness. A small background still remained, and thus an argon resonance at 77 keV was used to evaluate this near the ROI. This background is also expected to be flat in TOF.

Figure 2 shows the GAr and LAr event rates as a function of TOF and energy. The background rates are fit to a constant resulting in a background contribution relative to the signal in the ROI of about 0.14% for LAr and 7.1% for GAr, where the one-sigma uncertainties (dotted lines) are given by the flat fit to all background measurements.

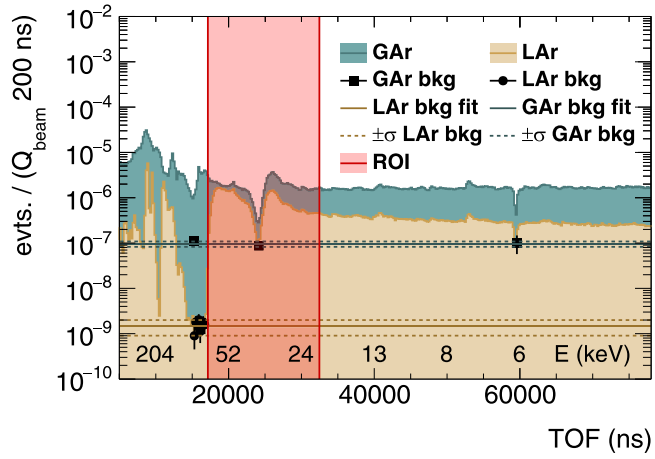

FIG. 2. The event rates and energy for a LAr and GAr filled target as a function of TOF. Filled points are the extracted background rates.

Long-term beam line stability. The cross section calculation relies on the proportional nature between neutrons detected and the total integrated beam current, yet, other than the ^{6}Li detectors at the end of the beam line, there is no monitor of the neutron flux once the proton beam strikes the tungsten target. Since gaseous and LAr data runs involve different target setups, the uncertainties associated with the neutron beam in the target hall, after the neutrons are created, are not canceled naturally in Eq. (2). To assess these uncertainties, event rates normalized by beam current were analyzed as a function of time for both air and LAr data, discussed below.

Air. The target was periodically run with air inside instead of liquid or gaseous argon. These air data, due to similar densities and neutron cross sections, were used as a surrogate for long-term beam line stability of GAr data. This assessment includes any systematic effects from changing atmospheric pressure. Three days of air data showed a daily modulation correlated closely to outside air temperature, and consistent across energies below, within, and above our ROI. Due to the close correlation to temperature, we suspect the effect is due to misalignment from the thermal expansion and contraction along the entire length of the beam line. The combined uncertainty on median air event rate is taken as an asymmetric systematic of +3.14% and −3.93% [21].

LAr. LAr data did not show the same modulation as the air data. A measurement of the event rate as a function of time for LAr includes event rate decrease from ice buildup on the Kapton windows and also the cuts used to remove periods of refilling. The combined uncertainty on median LAr event rate is taken as an asymmetric systematic of +0.69%, and −1.06% [21].

Target density. As described in the calibration section, this was measured with a systematic uncertainty of 1.3%.

After the selection cuts, several other systematic uncertainties were determined to be negligible, including those from nonlinearity between the beam intensity and CT measurement, dead time in the DAQ system [21], PMT afterpulsing [21], and contamination of the argon gas.

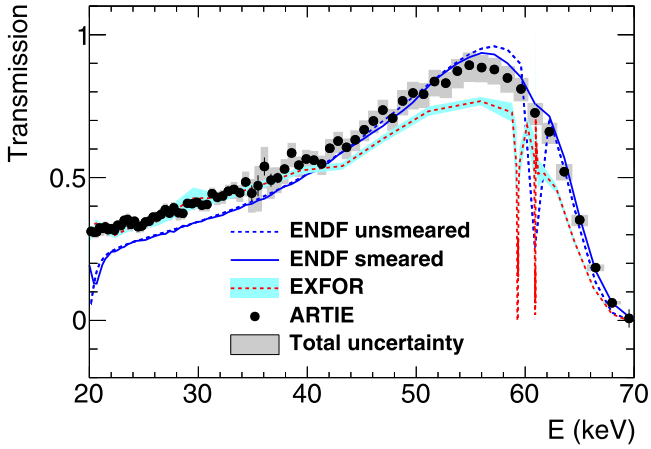

FIG. 3. The measured transmission of argon compared to EXFOR [14] and ENDF. The points are the central values and the bars represent the statistical uncertainty. The shaded grey regions are the total uncertainty, including systematics. For most energies, statistical error bars are smaller than the symbols.

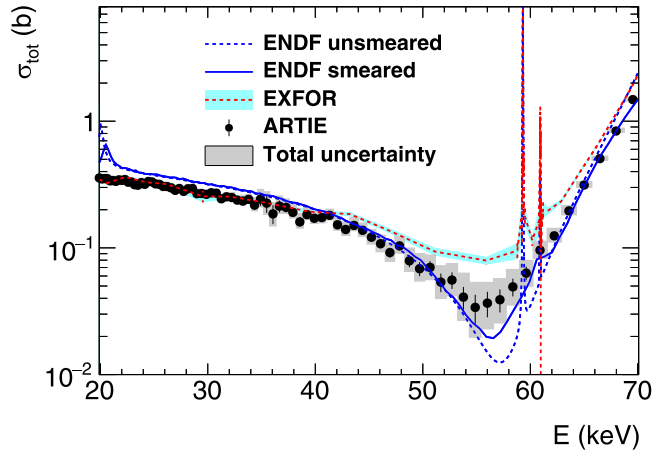

FIG. 4. Neutron-argon total cross section as a function of energy. Also shown are the EXFOR evaluation and the ENDF evaluation smeared by the ARTIE energy resolution.

The absolute energy calibration was limited by the statistical uncertainties on the fitted parameter $\delta(t_{\text{fit}}) = 29$ ns, and the contribution from $\delta(L_{\text{fit}}) = 0.064$ m was negligible. No systematic uncertainty for energy resolution was applied to the cross section results, which are reported here as a function of measured energy.

The total systematic uncertainties on transmission and cross section are estimated for each energy point by using a toy Monte Carlo simulation where all relevant parameters are allowed to vary simultaneously around their central values. The resulting spreads within the 68th percentile around the central-value measurements of transmission and cross section are taken as the total systematic uncertainties.

Conclusions. Using the TOF data and measured backgrounds, the transmission T is calculated from Eq. (2) and the cross section from Eq. (1). The central value of each TOF bin is converted to energy using Eq. (3). Figure 3 shows the transmission as a function of energy for the range 20–70 keV. The measured neutron-argon total cross section as a function of kinetic energy is shown in Fig. 4.

The dashed red and blue lines represent the EXFOR database [14] and ENDF evaluation, and the solid blue line is the ENDF prediction smeared by the ARTIE energy resolution. The beam energy resolution does not allow us to see the sharp features near 60 keV. It can be seen that, for energies below 40 keV, the data are in good agreement with the EXFOR database [13], while the ENDF evaluation shows slightly higher cross sections. Between 40 and 70 keV, ARTIE data are in better agreement with ENDF, confirming the existence of the cross section dip. As a cross-check of our experimental setup and analysis technique, the transmission for carbon was measured from data collected with two 0.125 ± 0.010 in. thick carbon (99.999% purity) disks [20] attached to the target while filled with GAr. There was good agreement between the measured $(0.73^{+0.03}_{-0.05})$ and predicted (0.72) transmission in the ROI with $\chi^2/\text{NDF} = 2.7/6$, which confirms the analysis methodology.

In conclusion, our results confirm a dip in the total cross section in the region of 50–60 keV. The point at 54.9 keV is found to have the lowest cross section of $\sigma = 0.0339 \pm 0.0087(\text{stat.})^{+0.0175}_{-0.0112}(\text{sys.})$ b. These results can now be used to reliably predict neutron transport to the level required in current and future experiments using liquid argon.

Work at UC Davis was supported by the U.S. Department of Energy (DOE) Office of Science under Award No. DE-SC0009999, and by the DOE National Nuclear Security Administration through the Nuclear Science and Security Consortium under Award No. DE-NA0003180. Support for LIP was from the Fundação para a Ciência e a Tecnologia, I.P., Project No. CERN/FIS-PAR/0012/2019. Major support was also provided by the U.S. Department of Energy through the Los Alamos National Laboratory. Los Alamos National Laboratory is operated by Triad National Security, LLC, for the National Nuclear Security Administration of U.S. Department of Energy (Contract No. 89233218CNA000001). Finally, we gratefully acknowledge the logistical and technical support and the access to laboratory infrastructure provided to us by LANSCE and its personnel.

[1] M. Antonello *et al.*, ICARUS at FNAL, Fermi National Accelerator Laboratory Report No. FERMILAB-PROPOSAL-1052, 2013 (unpublished).

[2] R. Acciarri *et al.*, Design and construction of the MicroBooNE detector, J. Instrum. **12**, P02017 (2017).

[3] B. Abi *et al.*, The single-phase protodune technical design report, arXiv:1706.07081.

[4] R. Acciarri *et al.*, Long-Baseline Neutrino Facility (LBNF) and Deep Underground Neutrino Experiment (DUNE) conceptual design report, Volume 1: The DUNE detectors at LBNF, arXiv:1601.05471.

[5] C. E. Aalseth *et al.*, DarkSide-20k: A 20 tonne two-phase LAr TPC for direct dark matter detection at LNGS, Eur. Phys. J. Plus **133**, 131 (2018).
[6] R. Ajaj *et al.*, Search for dark matter with a 231-day exposure of liquid argon using DEAP-3600 at SNOLAB, Phys. Rev. D **100**, 022004 (2019).
[7] K. H. Ackermann *et al.*, The GERDA experiment for the search of $0\nu\beta\beta$ decay in ^{76}Ge, Eur. Phys. J. C **73**, 2330 (2013).
[8] N. Abgrall *et al.*, The Large Enriched Germanium Experiment for Neutrinoless Double Beta Decay (LEGEND), in *Workshop on Calculation of Double-Beta-Decay Matrix Elements (MEDEX'17)*, 29 May–2 June 2017, Prague, AIP Conf. Proc. No. 1894 (AIP, New York, 2017), p. 020027.
[9] A. Friedland and S. Weishi Li, Understanding the energy resolution of liquid argon neutrino detectors, Phys. Rev. D **99**, 036009 (2019).
[10] A. M. Ankowski, P. Coloma, P. Huber, C. Mariani, and E. Vagnoni, Missing energy and the measurement of the cp-violating phase in neutrino oscillations, Phys. Rev. D **92**, 091301(R) (2015).
[11] S. Gardiner, Simulating low-energy neutrino interactions with MARLEY, Comput. Phys. Commun. **269**, 108123 (2021).
[12] D. A. Brown *et al.*, ENDF/B-VIII.0: The 8th major release of the nuclear reaction data library with CIELO-project cross sections, new standards and thermal scattering data, Nucl. Data Sheets **148**, 1 (2018).
[13] R. R. Winters, R. F. Carlton, C. H. Johnson, F. W. Hill, and M. R. Lacerna, Total cross section and neutron resonance spectroscopy for $n + {}^{40}$Ar, Phys. Rev. C **43**, 492 (1991).
[14] V. Semkova, N. Otuka, E. Dupont *et al.*, Towards a more complete and accurate experimental nuclear reaction data library (EXFOR): International collaboration between Nuclear Reaction Data Centres (NRDC), Nucl. Data Sheets **120**, 272 (2014).
[15] B. Abe *et al.*, Deep Underground Neutrino Experiment (DUNE), Far Detector Technical Design Report, Fermi National Accelerator Laboratory Report No. FERMILAB-PUB-20-025-ND, 2020 (unpublished).
[16] B. Abi *et al.*, Deep Underground Neutrino Experiment (DUNE), far detector technical design report, Volume IV: Far detector single-phase technology, arXiv:2002.03010.
[17] P. W. Lisowski, C. D. Bowman, G. J. Russell, and S. A. Wender, The Los Alamos National Laboratory spallation neutron sources, Nucl. Sci. Eng. **106**, 208 (1990).
[18] L. Zavorka, M. J. Mocko, P. E. Koehler, and J. L. Ullmann, Benchmarking of the MCNPX predictions of the neutron time-emission spactra at LANSCE, American Nuclear Society, 20th topical meeting of the radiation protection and shielding division of ANS, 2018.
[19] H. M. Roder, Liquid densities of oxygen, nitrogen, argon, and parahydrogen, NBS Technical Note 361 (Revised), 1974.
[20] Carbon (Graphite) (C) sputtering targets, https://www.lesker.com/newweb/deposition_materials/depositionmaterials_sputtertargets_1.cfm?pgid=car1.
[21] T. Erjavec, Understanding neutron transport for liquid argon rare-event searches, Ph.D. thesis, University of California Davis, 2024 (unpublished).
[22] A. Stamatopolous, P. Koehler, A. Couture, B. DiGiovine, G. Rusev, and J. Ullmann, New capability for neutron transmission measurements at LANSCE: The DICER instrument, Nucl. Instrum. Methods Phys. Res. Sect. A **1025**, 166166 (2022).
[23] P. Koehler (private communication).
[24] R. Mucciola, C. Paradela, G. Alaerts, S. Kopecky, C. Massimi, A. Moens, P. Schillebeeckx, and R. Wynants, Evaluation of resonance parameters for neutron interactions with molybdenum, Nucl. Instrum. Methods Phys. Res. Sect. B **531**, 100 (2022).